# A New Approach for the Assessment of Allergic Dermatitis Using Long Wavelength Near-Infrared Spectral Imaging

*Ken Nishino; Department of Computer Science and Engineering, Toyohashi University of Technology; 1-1 Hibarigaoka, Tempaku, Toyohashi 441-8580, Aichi, JAPAN*

*Toshiharu Fujiyama; Department of Dermatology, Hamamatsu University School of Medicine; 1-20-1 Handayama, Hamamatsu 431-3192, Shizuoka, Japan*

*Hideo Hashizume; Division of Dermatology, Shimada Municipal Hospital; 1200-5 Noda, Shimada 427-8502, Shizuoka, Japan.*

*Shigeki Nakauchi; Department of Computer Science and Engineering, Toyohashi University of Technology; 1-1 Hibarigaoka, Tempaku, Toyohashi 441-8580, Aichi, JAPAN*

## Abstract

*Imaging devices for long-wavelength near-infrared light (e.g., MCT, InGaAs) and hyperspectral imaging devices using these wavelengths have recently been developed. This range of wavelengths is especially effective for measuring the composition of objects because it includes the absorption spectra of molecular vibrations. In this study, long-wavelength near-infrared spectral imaging was used to evaluate allergic dermatitis. Allergic dermatitis can be caused by 2 types of hypersensitivity, immediate (type I) and delayed (type IV), which are activated by different mechanisms. However, both types of dermatitis are characterized by erythema and localized tissue swelling of the affected area, and it is therefore difficult to determine the type of allergic response by macroscopic inspection. Near-infrared spectral imaging has attracted attention as a non-destructive inspection method, but while several studies have focused on the detection of edema by near-infrared spectroscopy, the previously reported methods have not attempted to differentiate between different types of allergic dermatitis by detecting intracutaneous targets specific to the different activation mechanisms. This study aimed to develop a method for the assessment of allergic dermatitis by using the long-wavelength near-infrared spectrum to detect intracutaneous allergic type-specific targets. Such a method was realized by establishing a spectral classifier for the spectra of type I and type IV allergic dermatitis reactions. A spectral classifier was established from the spectral datasets of histamine-induced cutaneous reaction (immediate type) and contact hypersensitivity erythema elicited by squaric acid dibutylester (SADBE; type IV), and a canonical discriminant analysis achieved very accurate detection of normal skin and types I and IV allergic dermatitis (normal skin: 87.2%, histamine induced reaction: 71.0%, SADBE contact hypersensitivity: 95.8%). The classifier was next applied to spectral images of 2 other skin conditions, red flare activated by methyl nicotinate (normal skin) and metal allergy (type IV), and these validation datasets were also correctly classified: the red flare induced by methyl nicotinate was categorized as normal skin and the contact hypersensitivity activated by the metal allergy patch test was categorized as a type IV allergic reaction. These results suggest a possible application of near-infrared spectral imaging to the assessment of allergic dermatitis.*

## Introduction

According to the Gell and Coombs classification system, allergic dermatitis can be categorized as either type I (immediate type) or type IV (delayed type) based on its mechanism of development[1]. However, it is difficult to determine the causative type of hypersensitivity response by the visible information such as color and morphological characteristics of the affected area. Dermatologists therefore make a diagnosis using a combination of visual inspection, a medical interview, palpation, and their clinical experience, and they must sometimes rely on the results of skin biopsy, an invasive method. However, a skin biopsy requires anesthesia and carries the risks of infection and scar formation. A noninvasive inspection providing an objective evaluation index would therefore be highly beneficial as an alternative or precursor to a skin biopsy.

Hyperspectral imaging has been rapidly evolving in recent years as a nondestructive method for measuring the grossly invisible physical and chemical properties of objects. The light reflected from an object's surface is known to contain a great deal of information about its source. Many applications of spectroscopy and spectral analysis have been reported. A hyperspectral image, which is an image that has spectral data for each pixel, allows such spectroscopy and spectral analysis research to expand from a single-point measurement to visualization of the distribution of measured properties. Most recently, imaging devices for long-wavelength near-infrared light (e.g., MCT, InGaAs) and hyperspectral imaging devices using these wavelengths have been developed. This wavelength range is especially effective for measuring the composition of an object because it includes the absorption spectra of molecular vibrations. Therefore, this technique is a promising new nondestructive visualization method that could be applied in a wide variety of fields. In this study, long-wavelength near-infrared spectral imaging was used to evaluate allergic dermatitis.

The nondestructive and noncontact nature of optical measurements has long attracted research on their applications to biological targets. Hyperspectral imaging has the same advantages and has been reported be useful for evaluating dermatitis. Human skin pigments have spectral absorption properties in the visible range that produce human skin color[2]. The saturation levels of melanin and hemoglobin are the main contributors to skin color, and the red flare and melanin pigmentation developed by concentration of these pigments are actually quite important in derma-

tological diagnosis. In order to measure these human skin pigments, Tsumura et al. proposed a method for visualizing the distributions of melanin and hemoglobin from cross-polarized RGB images taken with polarization films installed on both the RGB camera and the illuminant[3].

On the other hands, there are many reports on the estimation of water content in vivo and the applications thereof, including the evaluation of lung edema, detection of interactions between atopic skin and pharmaceutical additives[4][5]. For the assessment of allergic dermatitis, Stamatas et al. proposed a method for evaluating erythema and edema in which oxyhemoglobin and water content distributions were visualized by visible and near-infrared spectral imaging[6][7][8]. However, the earlier studies allowed only the evaluation of red flare and swelling, which can be assessed by visible inspection and palpation. Therefore, the previously proposed techniques have not attempted to determine the type of allergic response (immediate or delayed), a key element in dermatologic diagnosis that at present can often be obtained only by a skin biopsy.

The purpose of this study was to develop a noninvasive method for assessing allergic dermatitis by using the long-wavelength near-infrared spectrum to detect intracutaneous allergic type-specific targets. As mentioned above, in general type I and type IV allergic dermatitis reactions have internal pathological differences. In particular, the erythema and edema in type I reactions are developed by IgE, mast cells, and particular chemical mediators, while type IV reactions are induced by macrophage and lymphocyte infiltration. Our plan to realize this measurement method was to develop a spectral classifier for the long-wavelength near-infrared spectra of the 3 skin conditions: normal skin and types I and IV allergic dermatitis. Briefly, near-infrared spectra are affected by the absorption properties of molecular vibrations of not only hydroxyl groups but also hydrocarbons. Furthermore, long-wavelength near-infrared spectra are very suitable for analyzing absorption properties as there is less light scattering in this range than at shorter wavelengths[9]. Long-wavelength near-infrared spectra of allergic dermatitis lesions may therefore contain information that is useful for discriminating among the different types. However, the spectral differences caused by oxy-hemoglobin accumulation and swelling alone will not suffice for the differentiation of type I and type IV dermatitis, as both types involve edema and erythema. For these reasons, any possible spectroscopic method for discriminating between these forms of dermatitis must rely on detection of intracutaneous allergic-type specific targets (e.g., accumulation of macrophages) that could aid in the differential diagnosis of allergic dermatitis.

## Materials and Methods
### Allergic Dermatitis

In this study, near-infrared spectra of erythematous artificially-produced urticarial (type I) and contact hypersensitivity (type IV) lesions were measured, and a classifier of near-infrared spectra in 3 skin conditions, 2 erythematous lesions and normal skin, was established to detect the spectral differences caused by the distinct immune responses. Previously existing techniques were not able to classify these spectra because these techniques focused only on the inflammation and swelling, whereas differential diagnosis of urticaria and contact hypersensitivity by near-infrared spectra will probably require detection of

spectral differences caused by the specific mediators of the immune responses. Near-infrared spectral images of 4 cases of artificially produced reddened skin were obtained in this study.

**Case 1**  Contact hypersensitivity induced by squaric acid dibutylester (SADBE)
**Case 2**  Urticaria induced by a histamine prick test
**Case 3**  Flare reaction induced by methyl nicotinate
**Case 4**  Contact hypersensitivity induced by a metal allergy patch test

Near-infrared spectral images from case 1 and case 2 were used as the training dataset for establishing the classifier. In this study, canonical discriminant analysis was used as the classification method. Case 3 and case 4 were used for validation. The flare reaction induced by methyl nicotinate should be classified as "normal skin" because it is not an allergic reaction. Case 4 should also be classified as contact hypersensitivity.

The induction of contact hypersensitivity by SADBE was performed on the left forearm of a 24-year-old man. The size of the application area was 3 cm x 10 cm. The hyperspectral image measurement was performed every few days from the early phase of the reaction to the late phase. For the measurement of case 2, the histamine prick tests were performed on the right forearms of 3 healthy adult men (1 aged 20-30 and 2 aged 30-40), and hyperspectral images of the resulting urticaria were obtained. The prick test patch Prick-Lancett (EWO Care AB, Gislaved, Sweden) was used with the histamine diluted to 1 mg/mL. For the measurement of case 3, a methyl nicotinate solution was applied to 2 square areas (1.5 cm x 1.5 cm) on the right forearm in order to produce a red flare. This experiment was performed on a 20-30-year-old male. In this rubifying procedure, methyl nicotinate solution was used at a concentration of 10%. For case 4, the metal allergy patch test was applied to the right forearm of a healthy adult male. Sixteen kinds of metal allergen from Torii Pharmaceutical Co., Ltd., (Tokyo, Japan) were used in this test. Patch tests with 17 substances (16 allergens and Vaseline) were left in contact with the arm for 48 hours. The substances included are described in Table 1.



**Figure 1.**  *Metal allergy patch test*

**Substances of the patch test**

| No. | Name | No. | Name |
|-----|------|-----|------|
| 1 | Aluminum chloride 2% | 10 | Potassium bichromate 0.5% |
| 2 | Chloroauric acid 0.2% | 11 | Chromium sulfate 2% |
| 3 | Stannic chloride 1% | 12 | Copper sulfate 1% |
| 4 | Ferric chloride 2% | 13 | Nickel sulfate 5% |
| 5 | Chloroplatinic acid 0.5% | 14 | Zinc chloride 2% |
| 6 | Palladium chloride 1% | 15 | Manganese chloride 2% |
| 7 | Indium trichloride 1% | 16 | Silver bromide 2% |
| 8 | Indium tetrachloride 1% | 17 | Vaseline |
| 9 | Cobalt chloride 2% | | |

## Hyperspectral image measurement conditions
### Near-infrared hyperspectral image

Figure 2 shows the measurement geometry of the near-infrared hyperspectral image measurement. A near-infrared line scan hyperspectral camera, Spectral Camera SWIR (Specim) is mounted in the measurement system, and the measurement target is placed on the movable plate under the camera. This camera has a 2-dimensional MCT sensor and can acquire an image in which the axes are position in the scanning area and wavelength. The spectral dataset of a linear scanning area obtained by measurement over a definite period of time can be reconstructed as a hyperspectral image because the measurement area plate slides with a constant velocity. The wavelength range was 909.35 nm to 2517.74 nm with 6.31 nm steps, the image resolution was 0.2 mm/pixel, the width of the scanning area was 320 pixels, and the height of the image was defined as up to the size of the measurement target. Three 150-W halogen lights were installed around the scanning area. The camera was calibrated using the Spectralon white reference.

### Visible hyperspectral image

To determine the relationships between the detection results and accumulation of oxyhemoglobin in the lesions, hyperspectral images in a range of visible wavelength were obtained in cases 2, 3 and 4. A multispectral imaging system, Nuance (CRi, Vis), was used for these measurements. The wavelength range of the hyperspectral image was 420 nm to 720 nm in 5 nm steps. A 500-W halogen light was used as the illuminant and the measurement was performed with 45/0 degree geometry. The measurement results are reported in the Discussion section.

## Results
### Measurement result

Reflectance spectra of both allergic dermatitis responses and normal skin were extracted from the measured hyperspectral images of cases 1 and 2 (contact hypersensitivity and histamine-induced urticaria), and spectral datasets were constructed. Masks of the dermatitis lesions were created manually, and the masks of the normal skin areas were defined automatically using the masks of the dermatitis lesions and the root mean square error from the predefined standard spectrum. The range of wavelengths was modified by a spline interpolation to 1000 nm to 2200 nm in 10 nm steps because the spectra outside of this range were too noisy due to the spectral sensitivity characteristics of the MCT sensor.
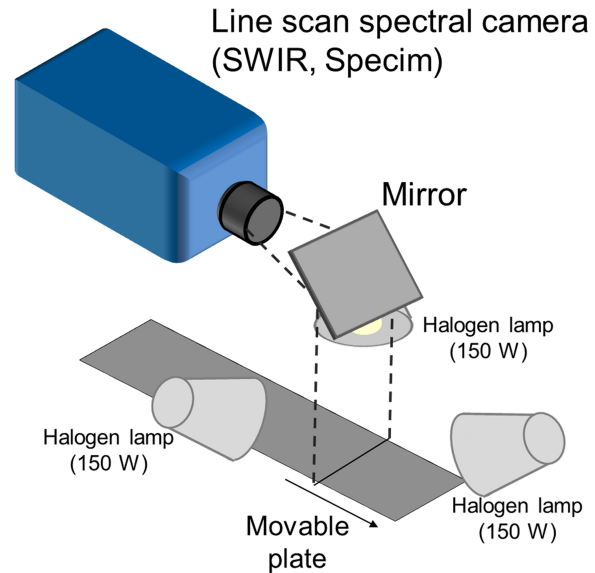


*Figure 2.* *Measurement geometry of the near-infrared hyperspectral image measurement. A near-infrared line-scan spectral camera SWIR (Specim) is mounted in the measurement system and the measurement target is placed on the movable plate under the camera.*

The average spectra of the measured absorbance spectra sets are shown in Fig.3. As shown in the figure, the absorbance spectrum of the SADBE-induced lesion is obviously different from that of the others. The cause of the spectral difference may be the severity of the edema rather than differences in the immune reaction, as the severities of the 2 dermatitis responses were clearly different.
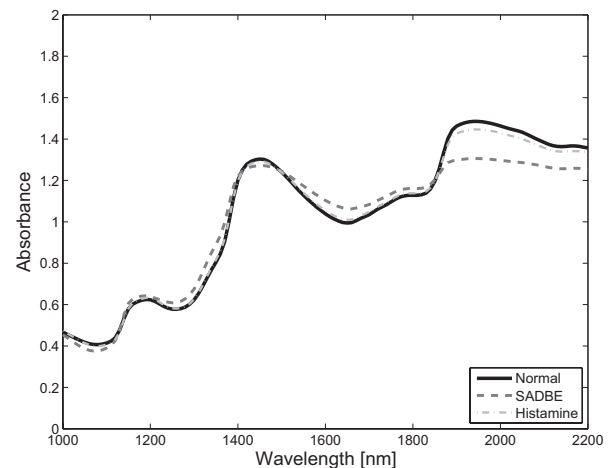


*Figure 3.* *Absorbance spectra of 3 skin conditions: contact hypersensitivity induced by SADBE, urticaria induced by histamine prick test, and normal skin.*

## Development of classifier

The purpose of this experiment was to obtain indices for independently evaluating the histamine-induced urticaria and SADBE-induced contact hypersensitivity. To that end, canonical

discriminant analysis was performed on the near-infrared spectra of both dermatitis lesions and normal skin. The canonical discriminant analysis creates a discriminant space based on maximizing the variations between subgroups. Therefore, if it is possible to classify these 3 conditions by projection of the near-infrared spectra to the canonical discriminant space, the canonical discriminant scores will allow independent evaluation of these dermatitis responses. In other words, such a result suggests that the discriminant vector detects some sort of spectral difference caused by the different immune reactions.

### Computational result

From the analytical point of view, the same number of spectra should be extracted from each hyperspectral image. However, the histamine-induced urticaria lesions were much smaller than the contact hypersensitivity lesions. Therefore, boot-strap resampling was applied to the datasets so that the numbers of extracted spectra would be the same. In total, 2000 spectra were extracted from each image (urticaria, contact hypersensitivity, normal skin in the urticaria images, and normal skin in the contact hypersensitivity images) to construct the training dataset. Before the canonical discriminant analysis, the multiplicative scattering correction (MSC) was applied to the reflectance domain and the corrected spectral reflectances were transformed to the spectral absorbance. The validation of the accuracy of the canonical discriminant analysis was performed by n-fold cross-validation. The spectral datasets consist of spectra extracted from 8 hyperspectral images (4 of urticaria and 4 of contact hypersensitivity). Therefore, the datasets were divided into 4 groups according to the hyperspectral images, and n-fold cross-validation was performed using n = 4. The canonical score map obtained by the canonical discriminant analysis is shown in Fig.4. The ovals in the figure show the equiprobability ellipses, the shafts of which were defined by the standard deviation under the 2-dimensional normal probability distribution assumption.
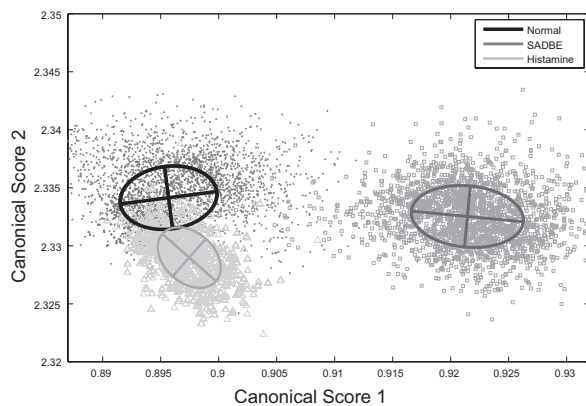


**Figure 4.** *Canonical score map. Canonical scores of all spectra were computed using the canonical discrimination function and the scores of each skin type were plotted on the canonical space. The ovals in the figure show the equiprobability ellipses, the shafts of which were defined by the standard deviation under the 2-dimensional normal probability distribution assumption.*

As shown in Fig.4, the spectral sets of the 3 conditions are clearly separated in the canonical discriminant space. Note that the directions of the score shifts from normal skin to hypersen-

**Rates of correct skin condition classification**

| Skin condition | Correct rate |
| --- | --- |
| Contact hypersensitivity | 95.8 % |
| Histamine-induced urticaria | 71.0 % |
| Normal skin | 87.2 % |
| Average | 85.3 % |

sitivity and normal skin to urticaria are nearly orthogonal. This result indicates that the canonical discriminant space allows the creation of independent evaluation indices for each dermatitis response. To obtain the evaluation indices, a quadratic Bayesian classifier for these 3 skin conditions was created on this space. The rates of correct classification are shown in Table 2. These were computed using leave-1-out cross-validation. As described in Table 2, classification accuracies of all conditions are much higher than the chance-level (33.3% ).

### Visualization result

The developed canonical discrimination function was applied to the spectral images to visualize their dermatitis lesions. Here, the near-infrared hyperspectral images used to construct training datasets were also used for visualization. The visualization results are shown in Fig.5. The posterior probabilities of dermatitis defined by the canonical score distributions in Fig.4 were computed for all pixels of the spectral images, and the dermatitis lesions were colored. An MSC and masking of the background were applied as preprocessing steps, and a median filter was applied after the probability computation. In this figure, a probability of contact hypersensitivity is colored red, a probability of urticaria is colored green, and other areas are not colored. As shown in Fig.5, the dermatitis lesions were detected perfectly.
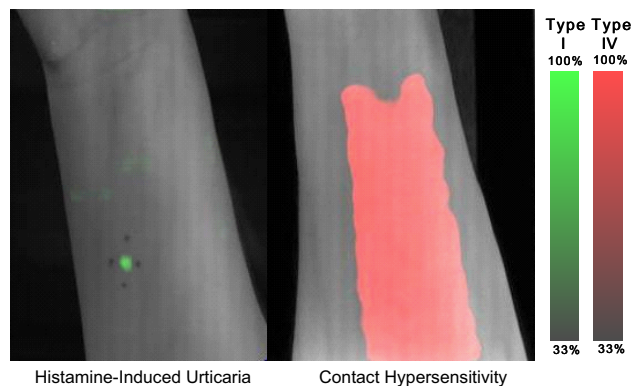


**Figure 5.** *Visualization result of histamine-induced urticaria and SADBE-induced contact hypersensitivity. The posterior probability of contact hypersensitivity is colored red, a probability of urticaria is colored green, and other areas are not colored.*

### Validation of the classifier

As described above, near-infrared spectra of healthy skin, skin with hypersensitivity, and urticaria can be classified very accurately by the system we developed. We suspected that the discrimination function detected some pathological difference between these dermatitis reactions other than inflammation and

swelling. Therefore, 2 additional cases, rubefaction by methyl nicotinate and a metal allergy test, were used to support this hypothesis. First, the canonical discrimination function (developed above) was applied to the near-infrared spectral image of rubefaction by methyl nicotinate. Methyl nicotinate induces a flare reaction with increased blood flow, but no edema is formed and no inflammatory cytokines are released, so this lesion should be classified as normal skin. Actually, no area of the spectral image in this case was classified as dermatitis.

Next, the discrimination function was performed on the spectral image of a metal allergy test, and the activated skin lesions were visualized. The visualization result is shown in Fig.6. As shown in the figure, 3 areas (= 3 different substances), those for cobalt chloride, nickel sulfate and zinc chloride, were detected as allergic dermatitis, which is in the same category as the SADBE-induced contact hypersensitivity. This is the correct classification result as a metal allergy is also a contact hypersensitivity reaction.
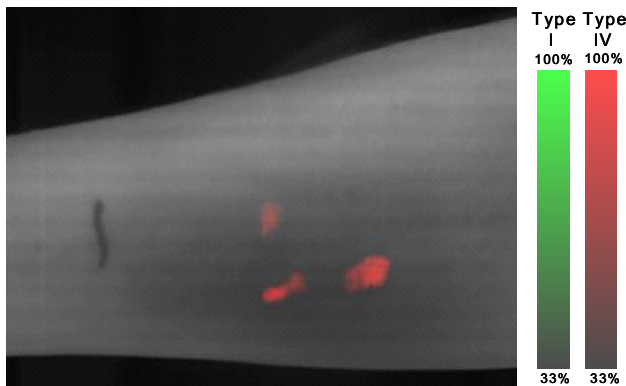


**Figure 6.** *Visualization result of metal allergy patch test. The posterior probability of contact hypersensitivity is colored red, a probability of urticaria is colored green, and other areas are not colored.*

## Discussions

As described in the first section, earlier studies of the evaluation of erythema focused on the spectral absorption properties of oxyhemoglobin and hydroxyl groups. However, these absorptions only allow the evaluation of visible elements such as inflammation and swelling. In contrast, our results described above suggest that the discrimination function that we developed may detect an internal component of allergic dermatitis. Therefore, in this section we compare the visualization maps to oxyhemoglobin and water content images to discuss what target was actually detected.

### *Comparison with oxy-hemoglobin accumulation*

To determine the relationship between the detection results and the accumulation of oxyhemoglobin, hyperspectral images of cases 2 and 4 were transformed into an $L*a*b*$ color space, as the $a*$ value is related to hemoglobin content[10]. A D65 spectrum illuminant was used for the color signal computation. The $a*$ channel images are shown in Fig.7. In these images, the skin area with accumulation of oxyhemoglobin appears light. In the case of metal allergy, only 3 patches were detected as contact hypersensitivity even though irritation with erythema appeared in many spots. Furthermore, in the case of histamine-induced urticaria, only the edematous area was detected as allergic dermatitis, while

the inflammation around the edema was not detected. Based on these results, the developed discrimination function detects spectral changes by edema rather than by erythema (accumulation of oxyhemoglobin).



(a) Urticaria induced by histamine
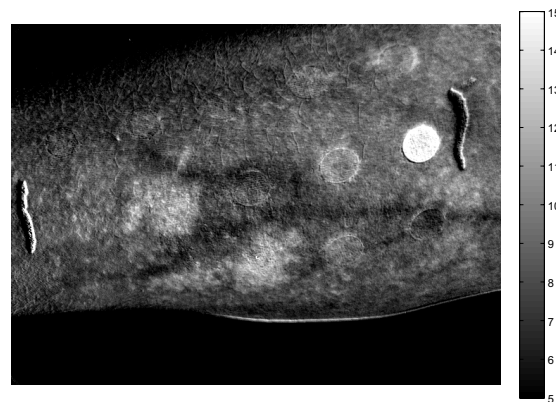


(b) Contact hypersensitivity induced by metal allergy patch test

**Figure 7.** *The $a*$ images of 7(a)) Urticaria induced by a histamine prick test and 7(b)) contact hypersensitivity induced by a metal allergy patch test*

### *Comparison with a water content image*

The results above indicate that the discrimination function used spectral characteristics of edema for discrimination between urticaria and contact hypersensitivity. As mentioned from the previous study, the absorption properties of the hydroxyl group, i.e., water content, figure strongly in the detection of the edema of allergic dermatitis[6][8]. Therefore, water content images were computed from the near-infrared spectral images to compare the allergic dermatitis visualization results and the corresponding water content distributions. In this analysis, a computation method for human skin moisture, subtraction of the spectral images at 1450 nm and 1060 nm, was used for the comparison because of

the wavelength range of the spectral image[11]. The computational water content image in the case of metal allergy is shown in Fig.8. As shown, the distribution of the water content is obviously different from the visualization result. The reason for the visualized water content accumulation is thought to be sweating caused by the stimulus of the test materials.
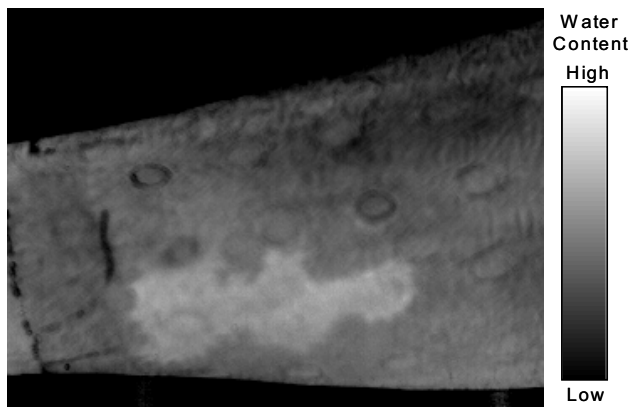


**Figure 8.** *Water content image of metal allergy. The water content was computed by the subtraction of the absorbances at 1450 nm and 1060 nm[11]. The area of highest water content does not match the detection result.*

## Conclusions

A long-wavelength near-infrared spectral imaging technique was applied to the assessment of allergic dermatitis in an attempt to detect and visualize intracutaneous differences caused by the activation mechanisms of different types of allergic dermatitis. The assessment method was established based on the spectral classification of 3 skin conditions, normal skin, and types I and IV allergic dermatitis. Near-infrared spectral images were measured over a wavelength range of 1000-2200 nm for 4 skin conditions: contact hypersensitivity induced by SADBE (type IV), urticaria induced by a histamine prick test (type I), flare reaction induced by methyl nicotinate (normal skin), and contact hypersensitivity induced by a metal allergy patch test (type IV). Training datasets for establishing the spectral classifier were extracted from the images of SADBE-induced contact hypersensitivity and histamine-induced urticaria (Fig.3). The canonical scores of these spectral datasets computed by the established canonical discrimination function made separate clusters as shown in Fig.4. The discrimination accuracies were also significantly high (Table 2), and the detected dermatitis lesions in the visualization results largely matched the macroscopic findings (Fig.5). Finally, this method was applied to 2 validation datasets (flare reaction induced by methyl nicotinate and metal allergy) with correct results for both classification and visualized lesions (Fig.6). Furthermore, an irritated spot (false-positive reaction) was not detected. It is apparent that the discrimination function detected some sort of internal allergic type-specific target that was neither hemoglobin pigment nor water content. These results suggest the potential utility of near-infrared spectral imaging for the assessment of allergic dermatitis. Specifically, this technique may be a useful tool for assisting the evaluation of metal allergy patch tests, as it can be difficult for the human eye to detect the false-positive/negative reactions. However, more subjects and cases should be evaluated to form a solid conclusion and develop a diagnostic tool. In our future work, we will apply this technique to other cases of allergic dermatitis to identify the detected substance.

## Acknowledgement

## References

[1] P.G.H. Gell and R.R.A. Coombs. *Clinical aspects of immunology.* Blackwell Science, 1963.

[2] E. Angelopoulou. The reflectance spectrum of human skin. Technical Report MS-CIS-99-29, GRASP Laboratory. Department of Computer and Information Science, University of Pennsylvania, 1999.

[3] N. Tsumura, M. Kawabuchi, H. Haneishi, and Y. Miyake. Mapping pigmentation in human skin from a multi-channel visible spectrum image by inverse optical scattering technique. *The Journal of imaging science and technology*, 45(5):444–450, 2001.

[4] S. Shibata, H. Ohdan, T. Noriyuki, S. Yoshioka, T. Asahara, and K. Dohi. Novel assessment of acute lung injury by in vivo near-infrared spectroscopy. *American journal of respiratory and critical care medicine*, 160(1):317, 1999.

[5] E. Dreassi, G. Ceramelli, L. Fabbri, F. Vocioni, P. Bartalini, and P. Corti. Application of near-infrared reflectance spectrometry in the study of atopy part 1. investigation of skin spectra. *The Analyst*, 122(8):767–770, 1997.

[6] G.N. Stamatas, B.Z. Zmudzka, N. Kollias, and J.Z. Beer. Non-invasive measurements of skin pigmentation in situ. *Pigment Cell Research*, 17(6):618–626, 2004.

[7] I.V. Meglinski and S.J. Matcher. Quantitative assessment of skin layers absorption and skin reflectance spectra simulation. *Physiological Measurement*, 23:741–753, 2002.

[8] G.N. Stamatas and N. Kollias. In vivo documentation of cutaneous inflammation using spectral imaging. *Journal of Biomedical Optics*, 12(5):051603, 2007.

[9] M.J.C. Van Gemert, S.L. Jacques, H. Sterenborg, and W.M. Star. Skin optics. *IEEE Transactions on Biomedical Engineering*, 36(12):1146–1154, 1989.

[10] B. Jung, B. Choi, A.J. Durkin, K.M. Kelly, and J.S. Nelson. Characterization of port wine stain skin erythema and melanin content using cross-polarized diffuse reflectance imaging. *Lasers in Surgery and Medicine*, 34(2):174–181, 2004.

[11] H. Iwasaki, K. Miyazawa, and S. Nakauchi. Visualization of the human face skin moisturizing-ability by spectroscopic imaging using two near-infrared bands. In *Eighth International Symposium on Multispectral Color Science (MCS06)*, pages 606203–1 – 606203–8, San Jose, California, USA, January 2006.

## Author Biography

*Ken Nishino was born in 1984. He received his Master Degree at the Toyohashi University of Technology, Japan in 2009. Currently He is a Ph.D course student at Toyohashi University of Technology, Department of Computer Science and Engineering. His research interests include color, multispectral imaging and human skin.*